IEEE Access
Multidisciplinary | Rapid Review | Open Access Journal

Received December 14, 2021, accepted December 22, 2021, date of publication December 28, 2021,
date of current version January 6, 2022.

Digital Object Identifier 10.1109/ACCESS.2021.3139269

A MIMO Antenna System Using Self-Decoupled EMSIW Dual-Beam Antenna Elements

PRIYA KUMARI, (Student Member, IEEE), AND SUSHRUT DAS, (Member, IEEE)
Department of Electronics Engineering, Indian Institute of Technology (ISM), Dhanbad, Dhanbad, Jharkhand 826004, India
Corresponding author: Priya Kumari (priyakumari91891@gmail.com)

This work was supported by the Department of Science and Technology, Government of India, through FIST Project.

ABSTRACT This paper presents a two-element MIMO antenna system using two dual-beam EMSIW antenna elements. The dual-beam pattern is achieved by creating two weak field areas using EMSIW. The antenna elements are placed in the weak field areas of each other, which results in −31.65 dB measured isolation between the two adjacent antenna elements. Different scenarios for the placement of the elements are predicted, one case is illustrated in this paper. The high isolation, omission of decoupling networks, and use of dual-beam antenna element make the antenna simple, compact, and suitable for MIMO applications.

INDEX TERMS Self-decoupling technique, eighth mode substrate integrated waveguide (EMSIW), dual beam antenna, mutual coupling.

I. INTRODUCTION

Substrate integrated waveguide (SIW) technology plays an important role in RF communication system design due to its numerous advantages [1]. For miniaturization purposes, fractional modes like half mode (HM) [2], quarter mode (QM) [3], eighth mode (EM) [4], and 64^{th} mode [5] are employed. Such a formation facilitates the placement of multiple antennas in a limited space. However, it also increases the mutual coupling between the elements, which directly affects the channel capacity and signal-to-noise ratio [6]. To increase the channel capacity and signal-to-noise ratio, MIMO technology can be employed. One of the major disadvantage of the MIMO system is the mutual coupling between the antenna elements. Therefore, several comprehensive studies were done in the past on the reduction of mutual coupling in MIMO systems. The introduction of double-layer metamaterial mushrooms [7], discrete mushrooms [8], and defected surface structure [9] between the elements reduce coupling by blocking the current rising from the exciting port. Providing an additional coupling path to cancel out the original one is another solution. It is done by using parasitic elements, decoupling structures [10], and neutralization lines [11]. However, these methods affect antenna compactness and increase fabrication complexity. Another way to reduce the correlation between antenna elements is the use of different diversity techniques [12], [13]. Spatial diversity occupies more space [14]. Pattern diversity techniques can be achieved by manipulating the electrical length [15] and exciting loop resonating modes [16]. It is noted that the number of available isolation enhancement techniques based on pattern diversity and SIW technology is limited [17]. The 'weak field area technique'for isolation improvements were introduced in [18], but it is applicable only for adjacent elements. In addition, [19] investigates a compact self-isolated MIMO system that uses a quarter-mode SIW cavity to achieve isolation of 18.5 dB without using any decoupling network, resulting in a narrow bandwidth of 60 MHz and gain (4.2 dB) at 3.5 GHz.

Multibeam antennas have the inherent ability to increase the data transfer rate. Butler matrix and lens type beamforming networks (BFN) are generally used to generate the multiple beams [20], [21], but they require a larger area. The quasi-yagi MIMO antennas in [22] employ the loop resonants mode to generate three directional beams. Various dual-beam microstrip antennas are also reported [23]–[25] that rely on the higher-order modes for generating the pattern. An mm-wave antenna [26], combining the SIW cavity (TE_{120}) mode and patch (quasi TM_{02}) mode, is also reported that shows a dual-beam nature. In [27], a 28 GHz single layer snowflake fractal antenna has been reported for dual-beam applications, but it has a low gain (3.2 dB).

In this communication, a two-element self-decoupled dual-beam MIMO antenna is presented for operation at 5.875 GHz. The SIW fractional mode concept based antenna elements generate a dual-beam pattern and two weak field areas. The antenna elements are placed in the weak field areas of each

The associate editor coordinating the review of this manuscript and approving it for publication was Giorgio Montisci.

other and hence do not require any additional decoupling network for isolation improvement. The high isolation, omission of decoupling networks, and use of dual-beam antenna element make the antenna simple, compact, and suitable for MIMO applications.

II. ANALYSIS OF THE ANTENNA ELEMENT

In this proposed work, the TM_{21} mode of a circular microstrip antenna is chosen because it has the inherent property of forming a conical beam. By combining the two reduced eighth modes of it, a dual-beam pattern has been formed. The antenna has been developed using HFSS v14 simulation software on a 1.575 mm thick, $\epsilon_r = 2.33$ and $\tan(\delta) = 0.0012$ Rogers 5870 substrate. No defects have been made on the ground to keep the antenna structure simple.

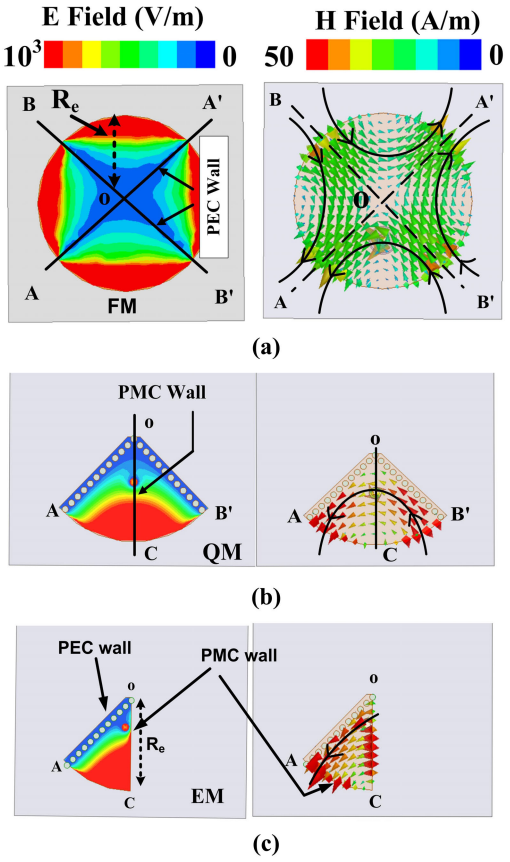

FIGURE 1. Plots of E-field (magnitude) and H-field (vector) distributions on (a) full-mode circular patch (FM), (b) quarter mode patch (QM), and (c) eighth mode patch (EM) at 5.89 GHz frequency.

The effective radius R_a (considering fringing effect) and actual radius R of a circular microstrip antenna, working in TM_{21} mode, can be related using (1) and (2) [28]; where c is the velocity of light in free space, k_{nm} is m^{th} zero of the derivative of the Bessel function of order n (m represents the radial mode and n represents the angular mode), and ϵ_r is the dielectric constant. For the given mode, $k_{nm} = 3.054$.

$$f_r = \frac{k_{nm}c}{2\pi R_a\sqrt{\epsilon_r}} \tag{1}$$

where,

$$R_a = R\sqrt{1 + \frac{2h}{\pi R\epsilon_r}[ln(\frac{\pi R}{2h}) + 1.7726]} \tag{2}$$

For $f_r = 5.89$ GHz, we get R = 15.28 mm. The optimized dimension of R is found to be $R_e =$ 15.7 mm, which is very close to the calculated value. The evolution of the eighth-mode of the substrate integrated waveguide cavity (EMSIW) from full-mode is depicted in Fig. 1. It reveals the TM_{21} mode of operation. The leakage loss through the gap between the vias has been avoided by choosing an appropriate pitch distance (p = 1.5 mm) and via diameter (d = 1mm) [29]. The existence of a perfect electric conductor (PEC) via wall along one edge and a perfect magnetic conductor (PMC) wall on the other edge makes the structure asymmetric with respect to its vertex and results in tilting of the beam towards the PMC wall when used as an antenna. This tilting of the beam has been utilized in this work to form the dual-beam.

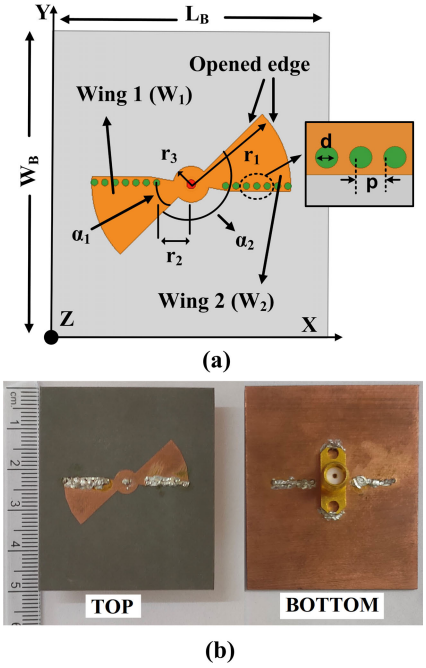

FIGURE 2. (a) Geometrical view and (b) top and bottom view of the fabricated antenna. $L_B = 40$ mm, $W_B = 47$ mm, $r_1 = 14.4$ mm, $r_2 = 5.2$ mm, $r_3 = 2.8$ mm, p = 1.5 mm, d = 1 mm, $\alpha_1 = 48.7°$ and $\alpha_2 = 180°$. Overall dimension of the PCB is 40 mm × 47 mm × 1.575 mm ($0.78\lambda_o \times 0.92\lambda_o \times 0.03\lambda_o$ at 5.89 GHz).

By arranging two miniaturized eighth mode SIW wings (W_1 and W_2), a dual-beam antenna has been formed, as shown in Fig. 2(a). The fabricated prototype is shown in Fig. 2(b). The radius r_1 and apex angle α_1 of the EMSIWs are optimized to achieve good impedance matching. The angle between the open (or short) edges of the two EMSIW is kept $\alpha_2 = 180°$ to maintain nearly identical beam gain. If $\alpha_2 \neq 180°$, two beams with different realized gain are formed. A conical beam pattern is formed if another pair of wings are added with $\alpha_2 =$ 90° [30], [31]. A broadside beam can be formed if the wings are arranged as [32]. The generated beams are

directed nearly towards the ± y-axis because the phase line of the proposed geometry is away from $\phi = 0°$ [33]. The simulated E-field distribution on the antenna (Fig. 3) reveals the existence of two weak field regions along the shorted sides of the EMSIW wings. The weak field regions are formed due to the existence of the metal via walls that short the current. The weak field regions facilitate the close placement of more antenna elements, maintaining high isolation between them. One such case has been presented in section III.

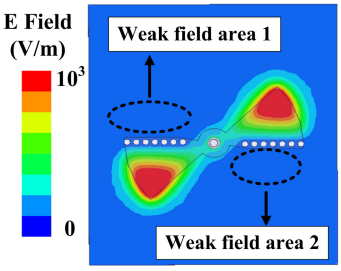

FIGURE 3. Simulated electric field distribution (magnitude) on the antenna at 5.89 GHz.

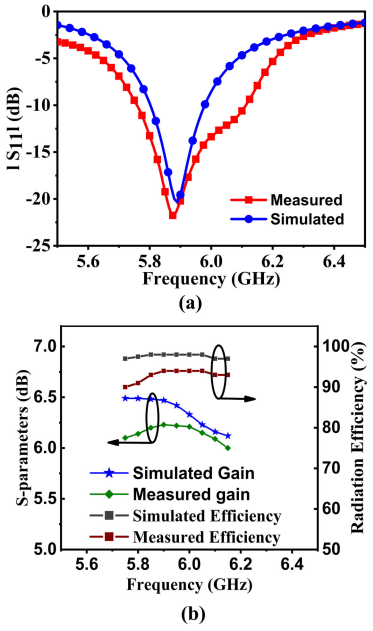

FIGURE 4. Simulated and measured (a) $|S_{11}|$, (b) gain and radiation efficiency of the antenna.

Comparison of the $|S_{11}|$ responses of the antenna (Fig. 4 (a)) shows measured and simulated 10 dB return loss bandwidths of 5.76-6.11 GHz and 5.8-5.98 GHz, respectively. Peak realized gain and radiation efficiency data are plotted in Fig. 4(b). Obtained simulated and measured peak realized gain are 6.47 dB at 5.89 GHz and 6.23 dB at 5.875 GHz, respectively.

The measured radiation efficiency of the antenna can be calculated using the relation (3) [34].

$$Efficiency = \frac{Gain(G)}{Directivity(D)} \tag{3}$$

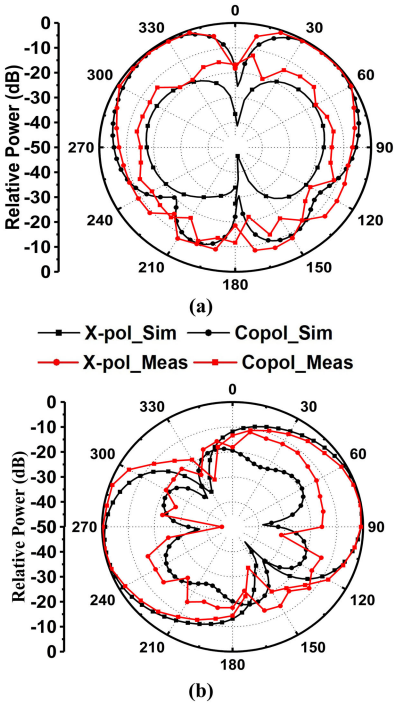

FIGURE 5. Normalized simulated and measured radiation pattern at (a) YZ plane (b) XY plane of an antenna element.

The gain (G) of the antenna can be measured using the standard gain comparison method, whereas the directivity (D) of the antenna can be measured using the pattern integration method. The pattern integration method requires that the E-field has to be measured in 3D at discrete sampling points, which is very time-consuming and expensive. Further, the corresponding measurement facility is also not available to us. Therefore, instead of measuring the directivity, we have considered the simulated directivity as the measured directivity. Since the directivity does not include the antenna losses, the measured directivity will be very close to the simulated directivity, and the simulated directivity can be considered as measured directivity [34]. This provides a measured radiation efficiency of 90%-94%, which is close to the simulated radiation efficiency (96%-98%). The slight degradation of the measured radiation efficiency is due to the fact that the measured gain is around 0.52 dB lower than the simulated gain.

The antenna has two distinct beams along $\theta = \pm 45°$ and $\phi = 75°$ and $-105°$ in simulation and $\theta = \pm 50°$ and $\phi = 80°$ and $-100°$ in measurement. The co- and cross-polarization radiation patterns at 5.89 GHz (simulated) and 5.875 GHz (measured) of the antenna in the E-plane and H-plane are plotted in Fig. 5. It reveals that the cross-polarization level is below -10 dB on both planes. The 0.56 dB and 0.52 dB differences in simulated and measured gains observed between the two beams are less than the prescribed limit of $\sim$ 2dB [35]. The measurements for the far-field responses of the proposed antenna are performed in an anechoic chamber as shown in Fig. 6.

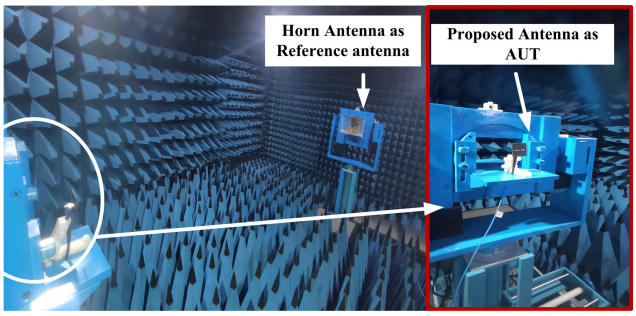

FIGURE 6. Setup for measuring the far-field of the proposed antenna element in an anechoic chamber.

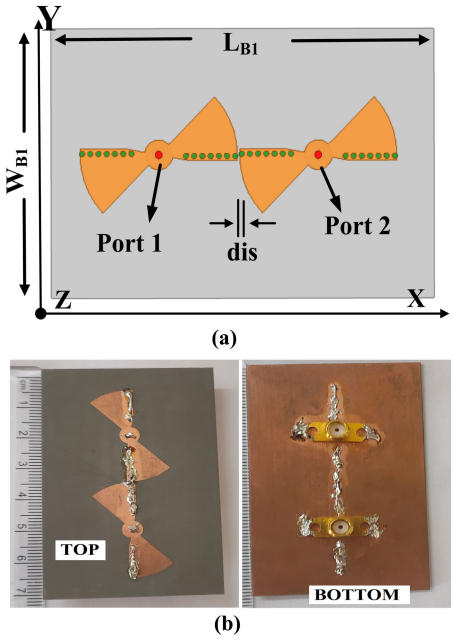

FIGURE 7. (a) Geometrical view, (b) top view and bottom view of the fabricated prototype. The dimensions are as follows: L_{B1} = 70 mm, W_{B1} = 44 mm, dis = 0.2 mm.

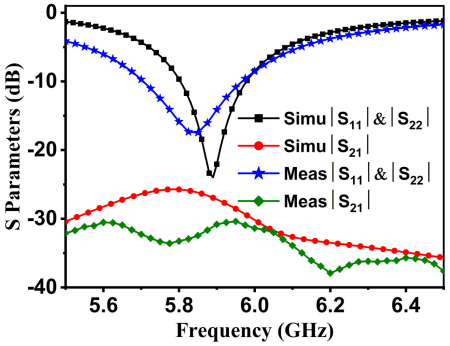

FIGURE 8. Simulated and measured S-parameters of the proposed MIMO antenna.

III. ANALYSIS OF MIMO ANTENNA

To form the MIMO antenna and analyze its self-decoupling property, two antenna elements are placed side by side along the X-axis in close proximity, as shown in Fig. 7 (a).

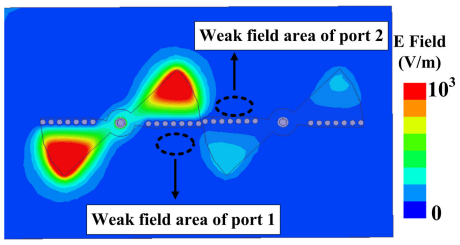

FIGURE 9. Simulated magnitude of electric current distribution of the adjacently placed antenna when port 1 is excited.

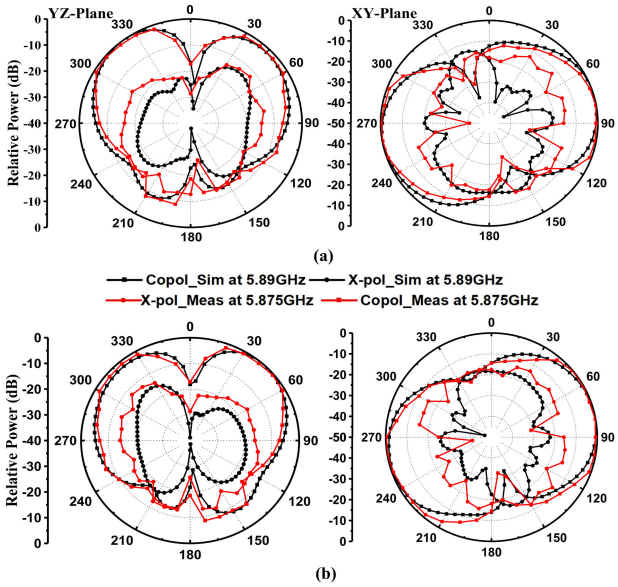

FIGURE 10. Simulated and measured radiation pattern of the proposed MIMO antenna, excited from (a) port 1 and (b) port 2.

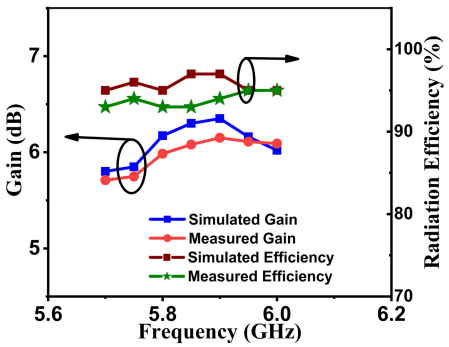

FIGURE 11. Simulated and measured maximum realized gain and radiation efficiency of the proposed antenna.

The fabricated prototype is depicted in Fig. 7 (b). The second antenna is placed in the weak field region of the first one, and vice versa. Thus, when both ports are excited, the beams from port 1 and port 2 fall on the weak field areas of the other, resulting in high isolation. In this work, only one weak field area is utilized. Other weak field areas can also be utilized by placing another element on them. The ground dimensions are optimized for better performance. Edge to edge distance (dis)

between the two elements is kept as 0.2 mm, which is the minimum distance required to avoid any fabrication error due to the finite resolution of the fabricating machine.

TABLE 1. Beam characteristics of the MIMO antenna.

	Forward Beam				Backward beam			
	Directions (°)		Gain(dB)		Directions(°)		Gain(dB)	
	Sim	Meas	Sim	Meas	Sim	Meas	Sim	Meas
Port 1	45	50	5.76	5.58	-45	-50	6.24	6.15
Port 2	45	50	6.2	6.05	-45	-50	5.74	5.62

Fig. 8 shows the comparison of simulated and measured frequency responses of the 2-element MIMO antenna. Isolations better than −27.2 dB in simulation and −31.65 dB in measurement are obtained with a respective 5.8-6 GHz and 5.71-5.96 GHz 10 dB return loss bandwidths. To analyze the isolation mechanism, the simulated E-field distribution (magnitude) on the antenna elements, when excited at port 1 is plotted in Fig. 9. During simulation, port 2 was match terminated. The figure reveals that the currents are mainly concentrated at the open corners of antenna 1, so a little current is coupled to port 2. The normalized co-polar and cross-polarization radiation patterns at 5.89 GHz (simulated) and 5.875 GHz (measured) are shown in Fig. 10. A slight change in the beam pattern is observed, which is due to the ground effect. The direction of the beams is near the ± y-axis. The cross-polarization levels are lower than −10 dB in both E- and H-plane. The simulated and measured beam directions and gain of the antenna are provided in Table 1. The simulated and measured realized gain and radiation efficiency curves are shown in Fig. 11. The measured efficiency of the proposed MIMO antennas has been measured using the same method described in section II. The measured radiation efficiency is around 95%, whereas the simulated radiation efficiency is around 97%. The MIMO antenna follows the characteristics of a single element with minor difference in the beam direction.

IV. DIVERSITY PERFORMANCE

This section presents the different MIMO parameters of the antenna to analyze its diversity performance. Fig. 12 (a) plots the envelope correlation coefficient (ECC) and diversity gain (DG) of the antenna. ECC and DG can be calculated from the far-field parameters using the relations provided in [36], [38]. The obtained ECC value is less than 0.04 and the diversity gain is greater than 9.98 dB, indicating that the channel has good diversity characteristics. The total active reflection coefficient (TARC) of the antenna can be calculated from the measured S-parameter values using [37] and is plotted in Fig. 12 (b). It shows the stable characteristics of the antenna when the phase angle between two ports varies from 0° to 180°.

The mean effective gain (MEG) is used to express the diversity performance of a multi-antenna system in terms of relative mean power levels between the signals supplied by each antenna branch [38]. S-parameters or 3-D radiation patterns can be used to depict the MEG for each port i of the MIMO antenna. The MEG is equal to half of the radiation efficiency if the statistical environment is uniform Rayleigh with equal horizontal and vertical polarization power densities. Based on the equations given below (4) and (5), MEG can be obtained by measured S-parameters values and plotted in Fig. 12(c).

$$MEG_i = 0.5\eta_{i,total} = 0.5[1 - \Sigma_{j=1}^{M}|S_{ij}|^2] \quad (4)$$

$$P_{MEG} = |MEG1 - MEG2| < 3dB \quad (5)$$

where M stands for the number of antennas, $\eta_{(i,total)}$ for total efficiency, i and j represent the exciting port and terminated port, respectively. The power ratio P_{MEG}, which is equal to the difference in the magnitude of MEGs, is determined for each branch with equivalent power levels. Therefore, for good diversity performance, the MEGs ratio should be approximate to unity (≈1), and their difference should not exceed ± 3 dB. It is observed from Fig. 12(c), that the proposed antenna fulfilling the criteria |MEG1/MEG2| ≈1 thus realizes good diversity performance.

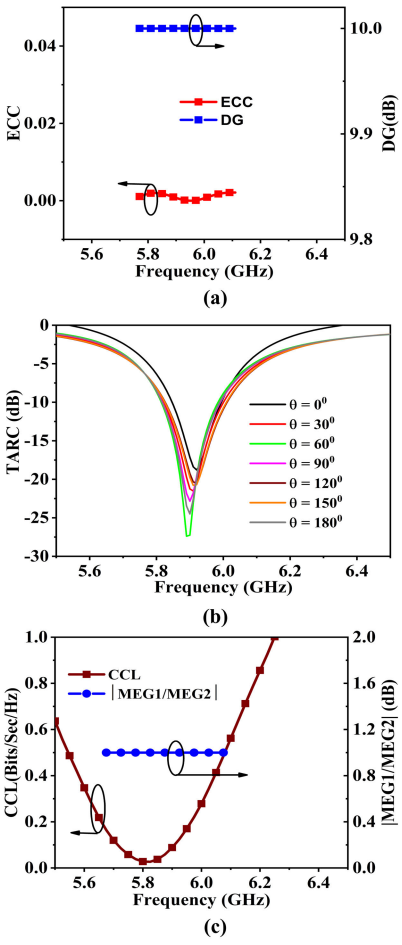

FIGURE 12. Calculated (a) ECC and DG, (b) TARC and (c) CCL and MEG ratio of the antenna.

The channel capacity loss (CCL) denotes the peak data rate at which the message can be continuously propagated with the least amount of loss. There is a linear relationship between

TABLE 2. Comparison of the proposed antenna with other SIW MIMO antennas.

Parameters	[7]	[8]	[17]	[39]	[40]	This Work
Total Size (λ_0^3)	0.96x0.96x0.18	1.2x1.2x0.11	0.41x0.41x0.04	0.75x0.83x0.02	1x0.76x0.72	1.37x 0.86x0.03
Edge to edge spacing (λ_0)	0.024	0.04	0.023	0.08	0.6	0.002
Frequency (GHz)	2.396-2.485	2.4-2.485	3.471-3.529 and 5.678-5.721	2.4, 5.15-5.85	5.15-5.85	5.71-5.96
Peak gain (dB)	4	7.1	2.7-2.85	3.2 and 5.8	6.2	6.15
Min. Isolation (dB)	42	35	18 and 22.7	20	30	31.65
Beam Direction	Broadside	Broadside	Broadside (30°tilted)	Broadside	Broadside	Dual-beam
Diversity Technique	Polarization	Polarization	Pattern and polarization	Polarization and shorted edges	Not reported	Pattern
Decoupling structure	Double metamaterial mushroom	Discrete mushroom	Metal strips	No	No	No

CCL and the number of elements. It may be estimated using the formulae (6) - (9), which are based on the measured S-parameter values [37].

$$CCL = -log_2 det(\psi^R) \tag{6}$$

where,

$$\psi_R = \begin{bmatrix} \rho_{11} & \rho_{12} \\ \rho_{21} & \rho_{22} \end{bmatrix} \tag{7}$$

Here,

$$\rho_{ii} = 1 - (|S_{ii}|^2 - |S_{ij}|^2) \tag{8}$$

$$\rho_{ij} = -(S_{ii}^* S_{ij} - S_{ji}^* S_{ij}) \tag{9}$$

Here, ψ^R is the correlation matrix for the two-port MIMO antenna system, and i and j represents the excited port and terminated port, respectively.

CCL must be less than 0.5 Bits/s/Hz for excellent MIMO performance in a multipath environment, assuming a high signal-to-noise ratio (SNR). Fig. 12(c) displays a plot of the proposed antenna's CCL data that meets the permitted limit. This is attributed to the enhanced isolation of the proposed antenna.

Table 2 outlines the advantages of the proposed antenna over the previously reported SIW-based MIMO antennas. It reveals that the proposed antenna has dual beam radiation as compared to the broadside beam of others. The antenna has higher gain compared to [7], [17], [39], [40] and better isolation than [17], [39], [40]. Though the antennas presented in [7] and [8] have 42-dB and 35-dB isolation, respectively, they use the metamaterial mushroom concept, which increases the volume and complexity of the antenna. [40] has a larger edge-to-edge spacing than this work. A compact solution is reported in [17], but it still gets the nominal isolation of 18 dB. In our approach, a self-decoupling theory is applied to achieve high isolation, and hence no extra decoupling network is required. The use of a dual-beam antenna element and the omission of decoupling networks in the structure make the antenna novel as compared to others.

V. CONCLUSION

This paper presents a 5.875 GHz self-decoupled dual-beam MIMO antenna using SIW technology. It is realized using the eighth mode of a circular microstrip antenna working with the TM_{21} mode, resulting in EMSIW. The EMSIW has a dual-beam pattern with two weak field areas, which assures −31.65 dB isolation between the two elements in close proximity; without using any decoupling methods. The dual-beam feature in MIMO configuration improves the performance and channel capacity by covering larger areas with a reduced number of antennas. ECC < 0.04, CCL < 0.5 Bits/s/Hz and MEGs ratio ≈1 have been observed, which insures good diversity performance. The antenna can be redesigned for another frequency by varying the radius r_1 and the apex angle α_1 of the EMSIW.

REFERENCES

[1] Q. Lai, C. Fumeaux, W. Hong, and R. Vahldieck, "Characterization of the propagation properties of the half-mode substrate integrated waveguide," *IEEE Trans. Microw. Theory Techn.*, vol. 57, no. 8, pp. 1996–2004, Aug. 2009.
[2] S. Agneessens and H. Rogier, "Compact half diamond dual-band textile HMSIW on-body antenna," *IEEE Trans. Antennas Propag.*, vol. 62, no. 5, pp. 2374–2381, May 2014.
[3] C. Jin, R. Li, A. Alphones, and X. Bao, "Quarter-mode substrate integrated waveguide and its application to antennas design," *IEEE Trans. Antennas Propag.*, vol. 61, no. 6, pp. 2921–2928, Jun. 2013.
[4] S. Sam and S. Lim, "Electrically small eighth-mode substrate-integrated waveguide (EMSIW) antenna with different resonant frequencies depending on rotation of complementary split ring resonator," *IEEE Trans. Antennas Propag.*, vol. 61, no. 10, pp. 4933–4939, Oct. 2013.
[5] S. Choudhury and A. Mohan, "Electrically small mode substrate integrated waveguide monopole antenna," *Electron. Lett.*, vol. 52, no. 8, pp. 580–581, Mar. 2016.
[6] X. Li and Z.-P. Nie, "Mutual coupling effects on the performance of MIMO wireless channels," *IEEE Antennas Wireless Propag. Lett.*, vol. 3, pp. 344–347, 2004.
[7] G. Zhai, Z. N. Chen, and X. Qing, "Enhanced isolation of a closely spaced four-element MIMO antenna system using metamaterial mushroom," *IEEE Trans. Antennas Propag.*, vol. 63, no. 8, pp. 3362–3370, Aug. 2015.
[8] G. Zhai, Z. N. Chen, and X. Qing, "Mutual coupling reduction of a closely spaced four-element MIMO antenna system using discrete mushrooms," *IEEE Trans. Microw. Theory Techn.*, vol. 64, no. 10, pp. 3060–3067, Oct. 2016.
[9] C.-Y. Chiu, C.-H. Cheng, R. D. Murch, and C. R. Rowell, "Reduction of mutual coupling between closely-packed antenna elements," *IEEE Trans. Antennas Propag.*, vol. 55, no. 6, pp. 1732–1738, Jun. 2007.

[10] L. Zhao and K.-L. Wu, "A decoupling technique for four-element symmetric arrays with reactively loaded dummy elements," *IEEE Trans. Antennas Propag.*, vol. 62, no. 8, pp. 4416–4421, Aug. 2014.
[11] S. Wang and Z. Du, "Decoupled dual-antenna system using crossed neutralization lines for LTE/WWAN smartphone applications," *IEEE Antennas Wireless Propag. Lett.*, vol. 14, pp. 523–526, 2015.
[12] S. P. Biswal and S. Das, "A planar triple band four element antenna system with polarization and pattern diversity for LTE/WLAN/DSRC applications," *Int. J. RF Microw. Comput.-Aided Eng.*, vol. 28, no. 4, Dec. 2017, Art. no. e21213.
[13] J. J. Liang, J. S. Hong, J. B. Zhao, and W. Wu, "Dual-band dual-polarized compact log-periodic dipole array for MIMO WLAN applications," *IEEE Antennas Wireless Propag. Lett.*, vol. 14, pp. 751–754, 2015.
[14] K.-L. Wong and J. Y. Lu, "3.6-GHz 10-antenna array for MIMO operation in the smartphone," *Microw. Opt. Technol. Lett.*, vol. 57, no. 7, pp. 1699–1704, Jul. 2015.
[15] C. F. Ding, X. Y. Zhang, C.-D. Xue, and C.-Y.-D. Sim, "Novel pattern-diversity-based decoupling method and its application to multielement MIMO antenna," *IEEE Trans. Antennas Propag.*, vol. 66, no. 10, pp. 4976–4985, Oct. 2018.
[16] S. S. Jehangir and M. S. Sharawi, "A miniaturized UWB biplanar Yagi-like MIMO antenna system," *IEEE Antennas Wireless Propag. Lett.*, vol. 16, pp. 2320–2323, 2017.
[17] A. Boukarkar, X. Q. Lin, Y. Jiang, L. Y. Nie, P. Mei, and Y. Q. Yu, "A miniaturized extremely close-spaced four-element dual-band MIMO antenna system with polarization and pattern diversity," *IEEE Antennas Wireless Propag. Lett.*, vol. 17, pp. 134–137, 2017.
[18] H. Lin, Q. Chen, Y. Ji, X. Yang, J. Wang, and L. Ge, "Weak-field-based self-decoupling patch antennas," *IEEE Trans. Antennas Propag.*, vol. 68, no. 6, pp. 4208–4217, Jun. 2020.
[19] B. Niu and J. Tan, "Compact self-isolated MIMO antenna system based on quarter-mode SIW cavity," *Electron. Lett.*, vol. 55, no. 10, pp. 574–576, May 2019.
[20] K. Xiang, F. Chen, Q. Chu, and M. J. Lancaster, "A broadband 3×4 Butler matrix and its application in multibeam antenna arrays," *IEEE Trans. Antennas Propag.*, vol. 67, no. 12, pp. 7622–7627, Dec. 2019.
[21] K. Liu, C. Zhao, S.-W. Qu, Y. Chen, J. Hu, and S. Yang, "A 3-D-printed multibeam spherical lens antenna with ultrawide-angle coverage," *IEEE Antennas Wireless Propag. Lett.*, vol. 20, pp. 411–415, 2021.
[22] S. S. Jehangir and M. S. Sharawi, "A wideband sectoral quasi-Yagi MIMO antenna system with multibeam elements," *IEEE Trans. Antennas Propag.*, vol. 67, no. 3, pp. 1898–1903, Mar. 2019.
[23] S. Liu, S. S. Qi, W. Wu, and D. Fang, "Single-feed dual-band single/dual-beam U-slot antenna for wireless communication application," *IEEE Trans. Antennas Propag.*, vol. 63, no. 8, pp. 3759–3764, Aug. 2015.
[24] J.-F. Li, Z. N. Chen, D.-L. Wu, G. Zhang, and Y.-J. Wu, "Dual-beam filtering patch antennas for wireless communication application," *IEEE Trans. Antennas Propag.*, vol. 66, no. 7, pp. 3730–3734, Jul. 2018.
[25] C. L. Chen, Y. X. Guo, and H. Wang, "Wideband symmetrical cross-shaped probe dual-beam microstrip patch antenna," *IEEE Antennas Wireless Propag. Lett.*, vol. 14, pp. 622–625, 2014.
[26] J. Y. Tan, W. Jiang, S. X. Gong, T. Cheng, J. Y. Ren, and K. Z. Zhang, "Design of a dual-beam cavity-backed patch antenna for future fifth generation wireless networks," *IET Microw., Antennas Propag.*, vol. 12, no. 10, pp. 1700–1703, Aug. 2018.
[27] H. Ullah and F. A. Tahir, "A novel snowflake fractal antenna for dual-beam applications in 28 GHz band," *IEEE Access*, vol. 8, pp. 19873–19879, 2020.
[28] J. Huang, "Circularly polarized conical patterns from circular microstrip antennas," *IEEE Trans. Antennas Propag.*, vol. AP-32, no. 9, pp. 991–994, Sep. 1984.
[29] D. Deslandes and K. Wu, "Accurate modeling, wave mechanisms, and design considerations of a substrate integrated waveguide," *IEEE Trans. Microw. Theory Techn.*, vol. 54, no. 6, pp. 2516–2526, Jun. 2006.
[30] C. Jin, R. Li, and A. Alphones, "Conical beam windmill-shaped array antenna design based on quarter-mode substrate integrated waveguide," *Prog. Electromagn. Res. Lett.*, vol. 39, pp. 1–8, 2013.
[31] J. Wang, X.-S. Yang, X. Ding, and B.-Z. Wang, "Topology optimization of conical-beam antennas exploiting rotational symmetry," *IEEE Trans. Antennas Propag.*, vol. 66, no. 5, pp. 2254–2261, May 2018.
[32] D. K. Karmokar, K. P. Esselle, and T. S. Bird, "An array of half-width microstrip leaky-wave antennas radiating on boresight," *IEEE Antennas Wireless Propag. Lett.*, vol. 14, pp. 112–114, 2014.
[33] W. D. Ake, M. Pour, and A. Mehrabani, "Asymmetric half-bowtie antennas with tilted beam patterns," *IEEE Trans. Antennas Propag.*, vol. 67, no. 2, pp. 738–744, Feb. 2019.
[34] Y. Huang, "Radiation efficiency measurements of small antennas," in *Handbook Antenna Technologies*, Z. N. Chen, D. Liu, H. Nakano, X. Qing, and T. Zwick, Eds. Singapore: Springer, 2016.
[35] A. Khidre, K. F. Lee, A. Z. Elsherbeni, and F. Yang, "Wide band dual-beam U-slot microstrip antenna," *IEEE Trans. Antennas Propag.*, vol. 61, no. 3, pp. 1415–1418, Mar. 2013.
[36] S. Blanch, J. Romeu, and I. Corbella, "Exact representation of antenna system diversity performance from input parameter description," *Electron. Lett.*, vol. 39, no. 9, pp. 705–707, May 2003.
[37] S. H. Chae, S.-K. Oh, and S.-O. Park, "Analysis of mutual coupling, correlations, and TARC in WiBro MIMO array antenna," *IEEE Antennas Wireless Propag. Lett.*, vol. 6, pp. 122–125, 2007.
[38] S. C. K. Ko and R. D. Murch, "Compact integrated diversity antenna for wireless communications," *IEEE Trans. Antennas Propag.*, vol. 49, no. 6, pp. 954–960, Jun. 2001.
[39] S. Yan, P. J. Soh, and G. A. E. Vandenbosch, "Dual-band textile MIMO antenna based on substrate-integrated waveguide (SIW) technology," *IEEE Trans. Antennas Propag.*, vol. 63, no. 11, pp. 4640–4647, Nov. 2015.
[40] S. Lemey, T. Castel, P. V. Torre, T. Vervust, J. Vanfleteren, P. Demeester, D. Vande Ginste, and H. Rogier, "Threefold rotationally symmetric SIW antenna array for ultra-short-range MIMO communication," *IEEE Trans. Antennas Propag.*, vol. 64, no. 5, pp. 1689–1699, May 2016.

PRIYA KUMARI (Student Member, IEEE) received the B.Tech. degree in electronics and communication engineering from the University College of Engineering and Technology (VBU), Jharkhand, India, in 2014, and the M.E. degree in wireless communication from BIT Mesra Ranchi, Jharkhand, India, in 2017. She is currently pursuing the Ph.D. degree with the Department of Electronics Engineering, Indian Institute of Technology (ISM) Dhanbad, Jharkhand, India. Her research interests include substrate integrated waveguide antennas and RF energy harvesting.

SUSHRUT DAS (Member, IEEE) received the B.Sc. degree (Hons.) in physics, in 1999, the M.Sc. degree in physics with specialization in electronics, in 2001, the M.Tech. degree in microwave engineering, in 2003, and the D.Phil. degree, in 2007. He joined the Indian Institute of Technology (Indian School of Mines) Dhanbad, Jharkhand, India, in 2007, where he is currently working as an Associate Professor with the Department of Electronics Engineering. He has guided nine doctoral thesis and published 57 technical articles in different reputed journals. He is also guiding eight doctoral thesis. He is also a PI and a Co-PI of different projects those are sponsored by the Government of India. His research interest include electromagnetics, antennas, and microwave circuits. He received the International Union of Radio Science (URSI) Young Scientist Award, Istanbul, Turkey, in August 2011.